Probing a planet from the subsurface to the atmosphere with infrasound data

Preprint · May 2024

DOI: 10.22541/essoar.171536007.73053488/v1

6 authors, including:

Marouchka Froment
Norsar
19 PUBLICATIONS **273** CITATIONS
SEE PROFILE

Quentin Brissaud
Norsar
48 PUBLICATIONS **747** CITATIONS
SEE PROFILE

Sven Peter Näsholm
University of Oslo
117 PUBLICATIONS **1,307** CITATIONS
SEE PROFILE

Antoine L. Turquet
Norsar
26 PUBLICATIONS **97** CITATIONS
SEE PROFILE

Probing a planet from the subsurface to the atmosphere with infrasound data

Marouchka Froment[1], Quentin Brissaud[1], Sven Peter Näsholm[1,2], Celine M Solberg[2], Tina Kaschwich[1], and Antoine Turquet[1]

[1]NORSAR
[2]Department of Informatics, University of Oslo

May 10, 2024

Abstract

The analysis of infrasound waves has a significant potential for retrieving a range of geophysical parameters across various scales, such as atmospheric structures, characteristics of surface and buried sources, and seismic velocity structures. This potential was recently showcased in infrasound studies that illustrated the ability to retrieve Earth's shallow velocities and Mars' near-surface atmospheric winds from remote acoustic observations. Consequently, infrasound is becoming an essential component of planetary missions, providing insights into the interiors and atmospheres of other terrestrial planets in the solar system. However, utilizing infrasound data requires efficient forward wave simulation techniques and an accurate description of waveform sensitivity to source and medium parameters. Even under ideal conditions, many inverse problems associated with infrasound-based probing are inherently ill-posed, necessitating regularization or other approaches to ensure reliable results. In this contribution, we highlight recent seismo-acoustic research findings, addressing atmospheric probing at both smaller and global scales, as well as innovative methods to accelerate infrasonic wave propagation modeling.

25·29 August 2024
inter.noise
NANTES FRANCE

Probing a planet from the subsurface to the atmosphere with infrasound data

Marouchka Froment*,[1] Quentin Brissaud,[1] Sven Peter Näsholm,[1,2] Celine M Solberg,[2]
Tina Kaschwich[1] and Antoine Turquet[1]

[1]NORSAR
Gunnar Randers vei 15, Kjeller, Norway

[2]University of Oslo
Department of Informatics, P.O. Box 1080, Oslo, Norway

ABSTRACT

The analysis of infrasound waves has a significant potential for retrieving a range of geophysical parameters across various scales, such as atmospheric structures, characteristics of surface and buried sources, and seismic velocity structures. This potential was recently showcased in infrasound studies that illustrated the ability to retrieve Earth's shallow velocities and Mars' near-surface atmospheric winds from remote acoustic observations. Consequently, infrasound is becoming an essential component of planetary missions, providing insights into the interiors and atmospheres of other terrestrial planets in the solar system. However, utilizing infrasound data requires efficient forward wave simulation techniques and an accurate description of waveform sensitivity to source and medium parameters. Even under ideal conditions, many inverse problems associated with infrasound-based probing are inherently ill-posed, necessitating regularization or other approaches to ensure reliable results. In this contribution, we highlight recent seismo-acoustic research findings, addressing atmospheric probing at both smaller and global scales, as well as innovative methods to accelerate infrasonic wave propagation modeling.

1. INTRODUCTION

Infrasound waves, low frequency, inaudible sounds below 20 Hz, have traditionally been used to monitor large man-made explosions and for verification of compliance with the Comprehensive Nuclear-Test-Ban Treaty [1]. Since low-frequency sound experiences little attenuation, it can propagate over large distances. When refracted and reflected back to the surface by atmospheric wind gradients, they provide unique constraints on atmospheric sources at a regional or global scale [2]. Beyond purely atmospheric propagation, the mechanical coupling between a planet's crust, its ocean, and its atmosphere allows waves to propagate across media (Fig. 1). Acoustic waves recorded in a planet's atmosphere, therefore, contain information about oceanic or underground sources and seismic velocities. In recent years, the number and quality of global infrasound array stations as well as the availability of open-source data and modeling tools has increased greatly [1]. The infrasound community has put great effort into investigating the sensitivity of infrasound waveforms to a wide range of medium and source characteristics [3].

*marouchka.froment@norsar.no

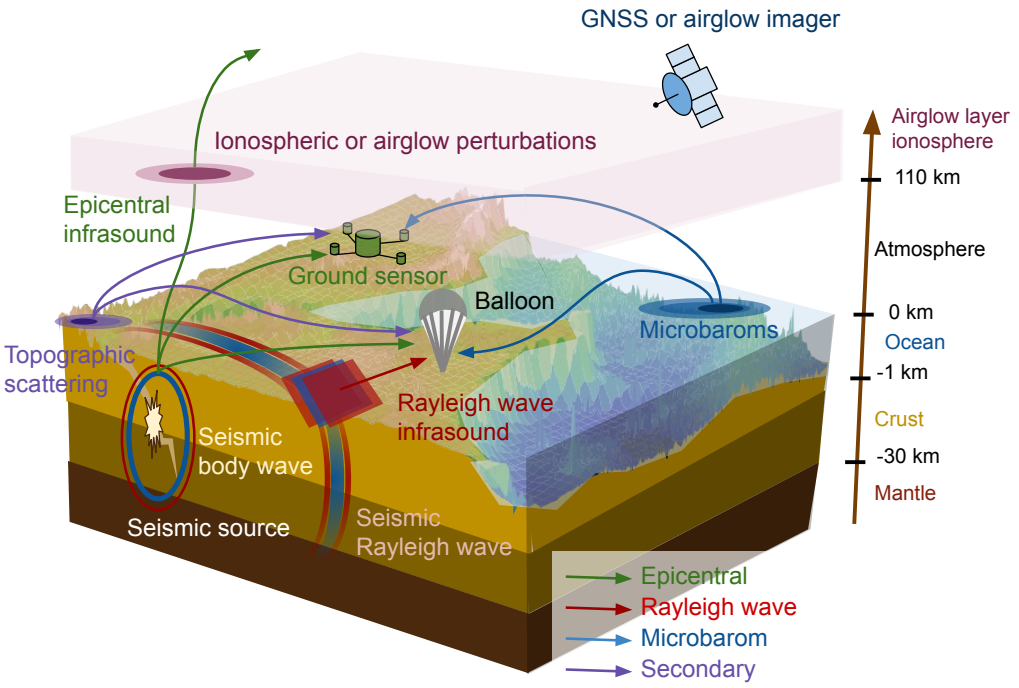

Figure 1: The seismo-acoustic wavefield on the Earth and infrasound sensor networks.

Traditionally, seismo-acoustic signals are detected using ground-based microbarometer arrays [1]. Due the relative scarcity of infrasound stations, seismic stations [4, 5] and Distributed Acoustic Sensing (DAS, [6]) have also been used to detect coupled infrasound. The detection of pressure waves in seismic records is often limited to high-amplitude pressure signals since most of the energy is reflected. Still, such data have been used to monitor meteor impacts [7], meteor shock waves and airbursts [8], as well as man-made explosions [9]. Innovative detection approaches have emerged, especially relying on Global Navigation Satellite Systems (GNSS, [10]) and airglow satellites (e.g., Thermosphere-Ionosphere-Mesosphere Energetics Dynamics (TIMED) mission [11]), and balloon platforms with microbarometers [12] or Inertial Motion Units (IMU, [13]).

Seismo-acoustic research has primarily focused on establishing simple regression models to correlate source characteristics, propagation paths, and waveform features such as amplitude or dominant frequency [14–18]. However, more recent work has successfully performed thorough inversion of source or medium properties by employing accurate weather or source models and physics-based modeling tools [19, 20]. In particular, the research community has developed a better understanding of the mechanical couplings between the subsurface, the ocean, the cryosphere, and the atmosphere, which are key for planetary exploration [21]. Previous reviews have proposed an overview of the infrasound applications and the main observations [3]. However, there is a need for a more technical examination of the methodology and challenges associated with infrasound-based inversion. Such an analysis is essential to evaluate its potential for applications beyond traditional infrasound fields, such as planetary exploration or weather modeling. In this contribution, we review recent research findings and their limitations to enhance our understanding of a planet's atmosphere and subsurface through infrasound sensing.

2. ATMOSPHERIC SENSING

On the Earth surface, the weather is mainly controlled by processes in the lower atmosphere, i.e., the troposphere (up to around 15 km altitude). Accurate tropospheric modeling is therefore key for robust weather forecasting. However, the lower atmosphere is also influenced by the dynamics of the middle atmosphere: the stratosphere (15–50 km altitude) and the mesosphere (50–90 km).

Compared to the troposphere, the middle atmosphere possesses a longer memory, which can influence the weather over extended periods, from months to entire seasons. Enhancing our understanding of middle-atmosphere dynamics and their interactions with other atmospheric layers is vital for advancing medium-range, i.e., sub-seasonal, weather forecasting [22]. Yet, the challenge lies in the inaccessibility of this region to traditional in situ measurement techniques, such as weather balloons. Consequently, one must turn to indirect methods of remote sensing to gain insight into the higher atmosphere. An emerging approach to probe the atmosphere relies on analyzing refracted infrasound waves, which can be generated by a variety of sources such as explosions, meteors, or ocean swell, and travel through the middle atmosphere (Fig. 1).

2.1. Stratospheric inversion

In seismic tomography, the main challenge with performing infrasound waveform inversion is to obtain robust source models, especially in terms of location and origin time. In contrast to a seismic medium, the atmospheric parameters vary over short time scales [23]. This greatly limits the sources that can be used for inversion and the temporal validity of a measured atmospheric state. For stratospheric inversion, man-made explosions and microbarom sources have primarily been used.

The great advantage of explosive sources is that locations and timing are generally well constrained and that finite source effects can be neglected at large distances from the source. Explosion-induced infrasound signals have been used to retrieve atmospheric profiles in regions of active mining and military activity primarily in the Nordics [5] and the United States [23]. Recent studies were able to measure stratospheric wind and temperature especially between 20 and 50 km altitude [22, 24, 25]. Importantly, these studies highlighted the lack of resolution of existing weather models over short spatial scales which can be resolved by infrasound measurements. To reduce the complexity of the inversion problem, arrival time, phase velocity, celerity, and backazimuth inputs are preferred to full waveforms (e.g., [25]). This allows one to neglect non-linear waveform distortion as waves are propagating at high-altitude [26] and avoid the calculation of an accurate source time function [19].

The altitude discretization of 1d atmospheric profiles can lead to a larger number of output parameters to invert for [24]. To regularize the inversion problem, authors have either used advanced sampling techniques such as particle swarm optimization [24] or reduced the number of output parameters by projecting atmospheric profiles onto a basis of Empirical Orthogonal Functions (EOFs, [25]). Nonetheless, explosions are costly and cannot be detonated globally for these purposes. Explosion-based infrasound inversion therefore provides only an atmospheric state solution at a given time. For example, repeating explosions over the same location also highlighted the strong variations in wind velocities over short time intervals [23].

In contrast to the scarcity of explosion data, microbarom signals are continuously generated and travel through the middle atmosphere [27]. Large-scale changes in stratospheric winds, such as those caused by a weakening or reversal of the stratospheric polar vortex, can be clearly observed in acoustic data [27]. Yet, the microbarom source mechanism is complex, also involving interference with ocean waves close to the coast or between storms. Modeling microbarom generation over extended regions requires accurate ocean wave models and the spatially distributed source makes it challenging to map microbarom infrasound recorded at a given time to specific propagation paths. Although traditional inversion procedures (e.g., gradient-based optimization) have not been used to map microbarom recordings to atmospheric winds, Vorobeva et al. [28] developed an innovative Machine Learning (ML) based approach to determine zonal polar-cap stratospheric winds based on microbarom infrasound data [28]. This model trains a neural network [29] to estimate the coefficients of Stochastic Delay Differential Equations along with estimates of the aleatoric and epistemic uncertainties of the model output. Quantifying uncertainties is key not only for inversion but also for interpreting "black-box" ML outputs.

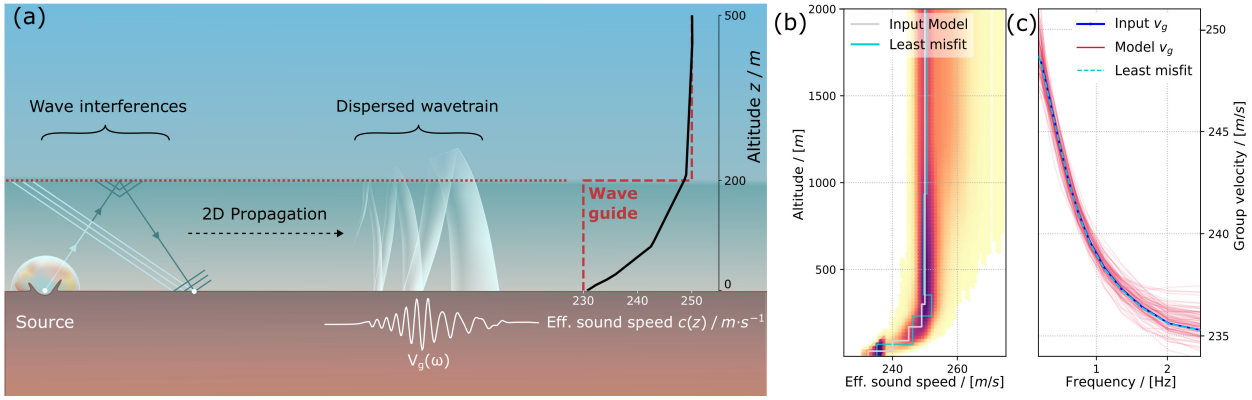

Figure 2: (a) Schematic representation of impact-generated infrasound propagation in a low-altitude waveguide on Mars. (b) Synthetic atmospheric model in grey and (c) associated synthetic group velocity curves in black. The colored background in (b) shows the probability density distribution of atmospheric models inverted from the synthetic group velocity curve of (c) using a MCMC method. (c) also shows 100 group velocity curves randomly picked from the posterior distribution in red and the solution with the least-misfit solution in blue.

2.2. Beyond the Earth

The methods mentioned above are not limited to the Earth. Recently, the InSight mission highlighted seismo-acoustics probing of the lower Martian atmosphere, or boundary layer. InSight landed on Mars in 2018 and also deployed a seismometer [30, 31]. The instrument operated until 2022 in combination with a meteorological sensor suite composed of wind and pressure sensors [32], which was indispensable to understand atmospheric noise in the seismic data.

Some of the InSight seismo-acoustic signals stem from local pressure perturbations, such as convective vortices and dust devils [33]. Others are coupled infrasound [34, 35] with undetermined sources. In addition, InSight detected infrasound following 6 meteorite impacts at 40 to 300 km distance [7, 36]. Some of these signals are associated with hypervelocity entry and dislocation of bolides, but the most prominent ones come from the atmospheric blast at the final surface impact. The location of these craters is known through a combination of seismic and satellite imagery analysis. Hence, Martian impact infrasound has a well-constrained source location and origin time.

Several of these infrasound arrivals show a clear dispersion between 0.5 and 4 Hz, signifying propagation in a near-surface waveguide, as observed on Earth [37, 38]. On Mars, such a waveguide arises at night due to the rapid radiative cooling of the surface, which causes an increase in sound velocities in the 500 to 1000 m above the surface, and can be further enhanced by seasonal winds [39]. Xu et al. [40] proposed an analytical model of this guided infrasound using compliance theory. They show that the dispersion relation depends on the vertical profile of effective sound speed, combining temperature and wind contribution. Recent results suggest that the group velocity of impact infrasound as measured by the seismometer can be used to invert the effective sound speed and winds in the first two kilometers of the Martian atmosphere [41, 42]. Due to the sparsity of the data and in order to quantify the uncertainty of the retrieved models, a Bayesian Markov chain Monte-Carlo inversion approach is chosen in this case, as shown in Fig. 2.

3. SUBSURFACE AND SEISMIC SOURCE SENSING

Seismic sources release energy as seismic waves, i.e., body and surface waves, which then couple to the surface and excite acoustic waves (seismic propagation paths in Fig. 1). Such acoustic waves are generally categorized into three types [3]: Epicentral infrasound excited at the epicenter and propagating spherically from the source [43], Rayleigh-wave infrasound generated by seismic Rayleigh waves, which propagate almost as plane waves vertically from the surface [21],

and secondary infrasound typically generated by surface waves traveling across topography and propagating spherically from the secondary source location [44].

3.1. Source parameter inversion

Epicentral infrasound generated by upward-propagating seismic body waves at the epicenter is a proxy for surface amplitude and therefore faulting type and history [45]. Early infrasound studies investigated the links between earthquake magnitude, infrasound peak amplitude, and frequency [43]. However, the amplitude and period are sensitive to a variety of source and path effects, including source depth, focal mechanism, crustal and mantle velocity, topography, and atmospheric wind gradients. Recent studies demonstrate that focal depth and focal mechanisms can be estimated from local [20] and global [46] epicentral and Rayleigh wave infrasound. Additionally, high-altitude Total Electron Content (TEC) perturbations excited by earthquake acoustic waves (the ionospheric layer in Fig. 1) are associated with a specific faulting mechanism [45].

Epicentral ground amplitude is typically retrieved by back-projecting pressure, or integrated pressure, amplitude recorded at ground-based arrays along their corresponding backazimuth [47]. Accurately capturing the propagation path is essential to properly retrieve ground shaking locations. Successful inversion benefited from favorable wind conditions associated with simple propagation paths, such as stratospheric waveguides [46, 48]. This ensures that amplitude and polarity estimates from distant recordings are not too corrupted by wave scattering along the propagating path caused, for example, by gravity waves [20]. Along the same line, the relative ground shaking intensity could be retrieved by projecting the TEC peak amplitudes from the Ionospheric Detection Point (IDP) to the ground level [10]. TEC data can be particularly useful, as GNSS networks are generally dense in populated areas around the world. However, the IDP is challenging to define since TEC recordings are integrated measurements of the electron density along the satellite line of sight in the ionosphere, and IDPs can vary from 150 to 300 km altitude [10].

Constraining the focal depth and the focal mechanism requires accurate amplitude and period predictions. Full-waveform simulations together with Monte-Carlo Markov Chain sampling of the source parameter space produced accurate predictions of yield or focal depth [18, 19] and focal mechanism [20]. In particular, the joint inversion of seismic and epicentral infrasound phases as recorded by an infrasound sensor was key to constrain the focal depth for shallow sources [18, 20, 49] since the amplitude ratio of both phases is highly sensitive to the source depth [50]. Note that recordings of the pressure associated with a seismic Rayleigh wave can be highly valuable by itself for constraining an earthquake magnitude in the vicinity of the epicenter, where seismic records are typically clipped [51]. Although infrasound waves are sensitive to finite source effects and their rupture velocity, no formal inversion of these seismic parameters has been performed due to the prohibitive computational cost of coupled seismo-acoustic simulations [45].

3.2. Subsurface structure inversion

Measuring and modeling Rayleigh wave infrasound waveforms recorded at ground-based sensors can provide a direct assessment of subsurface velocities, as done in surface-wave tomography [51, 53]. The pressure perturbation caused by a seismic Rayleigh wave is a scaled copy of its seismic counterpart [51], such that $A_i = \rho_a c_a A_s$, where A_i is the infrasound amplitude, A_s the vertical ground velocity amplitude, ρ_a the atmospheric density, and c_a the acoustic velocity. Yet, ground-based pressure inversion is generally not needed since seismic instruments are more sensitive to ground velocity than microbarometers, and since seismic networks are more dense than infrasound networks. Pressure recordings of seismic waves are of great value when instruments are deployed in the upper atmosphere, such as at balloons or low-altitude satellites, and do not require any ground-based deployments or when seismic instruments are lacking. Since acoustic wave dispersion below 20 Hz is insignificant up to high altitudes [21], seismic Rayleigh wave dispersion curves can then be directly extracted from upper atmospheric pressure records [21].

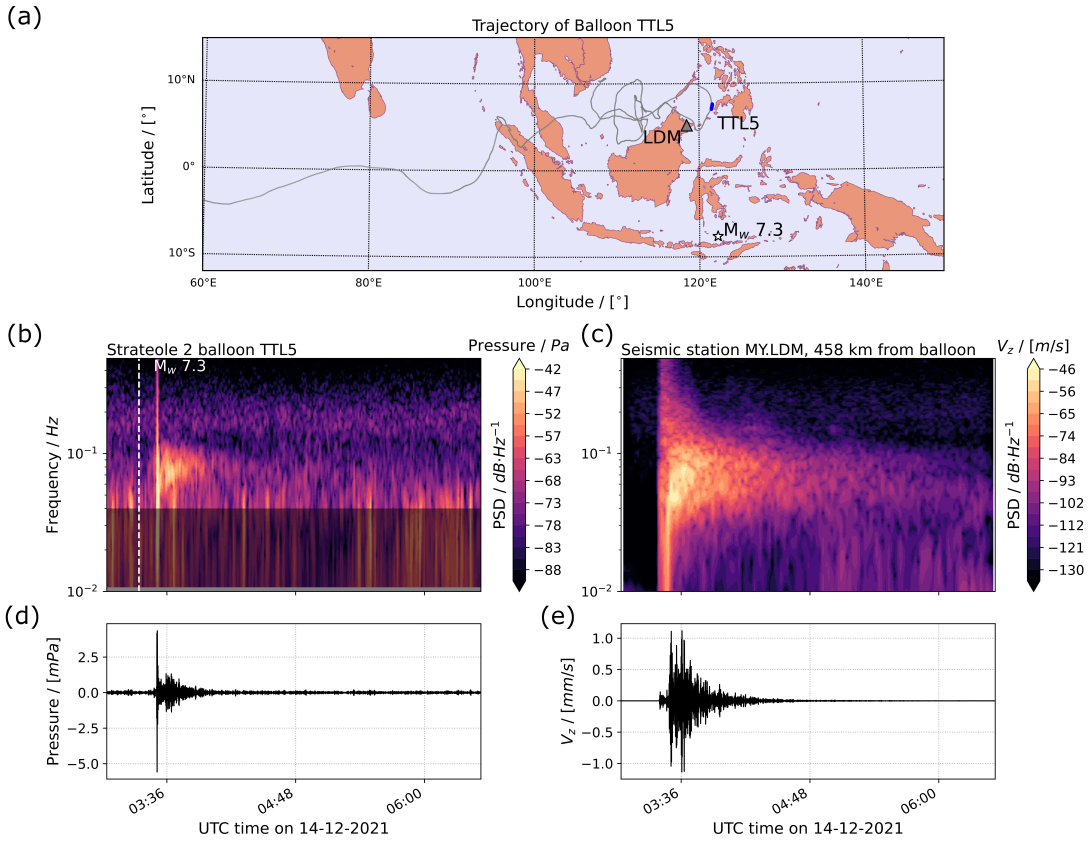

Figure 3: Signals from the $M_w = 7.3$ Flores sea earthquake, 14 December 2021 [52]. (a) position of the Strateole2 TTL5 balloon at the time of the event in blue, the epicenter and a nearby seismic station. (b) Spectrogram and (d) TTL5 pressure time series. The signal in the grey spectrogram area is filtered out to remove noise due to vertical balloon oscillation. Time series have been band-pass filtered between 0.05 and 0.1 Hz. (c) Spectrogram and (e) time series of the vertical velocity recorded at the LDM seismic station. The same filter has been applied to time series as for pressure data. The dispersion of the Rayleigh wave is visible in the pressure and velocity spectrograms.

Recent studies have offered glimpses on how to leverage balloon pressure data to perform seismic tomography. By shifting the infrasound records from a balloon platform in time to account for the acoustic travel time, both Brissaud et al. [21] and Garcia et al. [52] were able to extract average group velocity estimates for the surface Rayleigh waves. As an example of such dispersion studies, Figure 3 shows the signals recorded by a balloon and a nearby seismometer during the 2021 $M_w = 7.3$ Flores sea earthquake and reported by Garcia et al. [52]. The Rayleigh wave dispersion is visible in each spectrogram. These results demonstrated that the average crustal velocities can be extracted from Rayleigh wave infrasound. However, both studies benefited from accurate sources location and origin time model priors. Without a seismic catalog, both the source and subsurface parameters will have to be inverted jointly, as described in Fig. 4. Garcia et al. [52] suggested that using both S and Rayleigh wave arrival times in infrasound records can provide strong constraints on source parameters (Fig. 4b).

At higher altitudes, earthquake infrasound in ionospheric or airglow layers was primarily detected in the vicinity of the epicenter (< 500 km, [10]). Rayleigh waves have also been observed in TEC data from large earthquakes such as the 2011 Tohoku earthquake [54] with magnitudes generally above $M_w = 7$ [10]. TEC signatures of Rayleigh waves are also sensitive to average crustal and mantle structures as illustrated by observations above sedimentary basin [55] or above the the Indian subcontinent [56]. Yet, dispersion curves are challenging to extract in TEC data owing to the signals' low SNR at high frequencies. Most of the observed energy corresponds to the

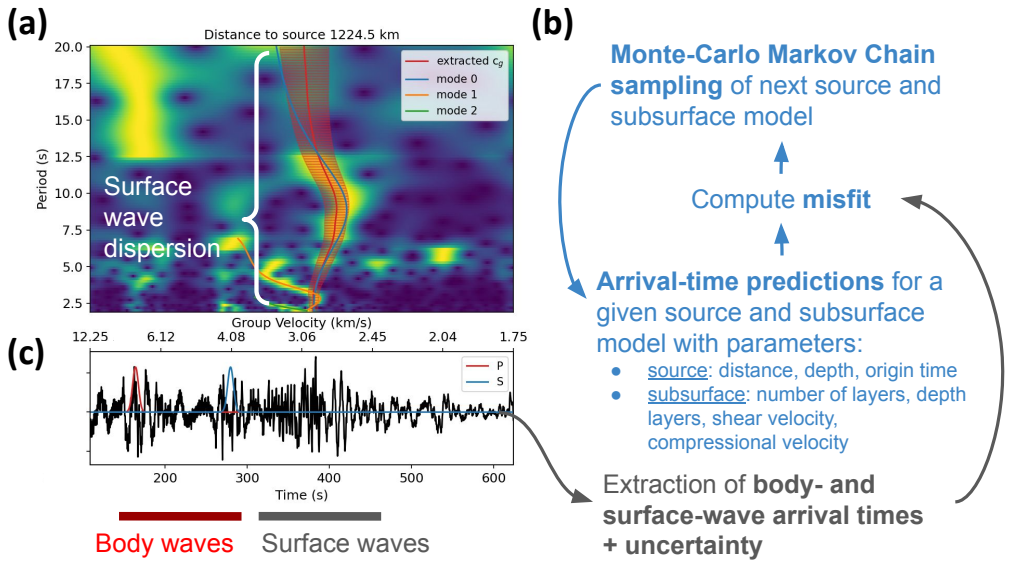

Figure 4: Subsurface structure inversion using balloon pressure data. (ac) Synthetic seismically-generated pressure, recorded at 1225 km from a 15 km reverse-fault seismic source, convolved with real balloon noise represented as (a) spectrogram vs period, in s, and time since the event, in s, and (c) pressure, in Pa, vs time since the event, in s. In (a), Theoretical Rayleigh wave arrival times are shown for the fundamental mode (blue), first higher mode (orange), and second higher mode (green) along with an example of Rayleigh wave dispersion curve extracted from the spectrogram (red) and its uncertainty (shaded red).(c) shows arrival time uncertainties for P wave (red) and S wave (blue). (b) Inversion workflow using Monte-Carlo Markov chain sampling.

resonant modes of the atmosphere which correspond to the lowest frequencies of the Rayleigh wave dispersion curves, known as Airy phases [57]. Therefore, although there were successful attempts to retrieve tsunami waveforms from TEC data recorded after the Tohoku earthquake [58], the inversion of crustal or mantle seismic velocities has never been performed.

4. CHALLENGES AND FUTURE DIRECTIONS

Despite many recent studies demonstrating the unique potential of infrasound-based inversion to constrain both atmospheric and subsurface media, they also highlight key challenges: **(i)** instrument design and noise, **(ii)** lack of observations, **(iii)** 3d global scale modeling, and **(iv)** ill-posedness and uncertainty propagation in the inversion process.

(i) The instrument and environmental noise at infrasound ground arrays is generally well characterized and the array aperture is often large enough to produce high signal-to-noise ratio beams [59]. However, both balloon and high-rate GNSS data show complex contributions of several noise sources [60]. In particular, in the case of balloon-borne sensors, noise models poorly capture the vortex shedding resulting from balloon motion and the mechanical response to local turbulence or impeding acoustic waves. Additionally, since the balloon payload is small, the number of pressure sensors is limited and no study has yet optimized beamforming capabilities based on known infrasound noise conditions. Hence, it can be difficult to discriminate between signal and noise, especially below 1 Hz [61]. This is particularly challenging when using differential barometers or Inertial Motion Units (IMUs, [13]) which are highly sensitive to small balloon accelerations. Nonetheless, recent theoretical efforts [62] have shown that the vertical response of superpressure balloons to impeding acoustic waves can be modeled and removed from IMU data.

(ii) For airglow and TEC data, a main challenge is to identify the Ionospheric Detection Points (IDPs) and to interpret the dispersion of the ionospheric waveforms, because these are integrated quantities along the satellite line of sight [10]. Kakinami et al. [63] simultaneously retrieved IDPs

and source location by stacking TEC arrivals observed across a GNSS network assuming a constant infrasound celerity [63]. Since the acoustic celerity varies with the launch angle, incorporating the IDP uncertainty can regularize the Bayesian inversion, especially for small datasets.

Regarding atmospheric sensing with infrasound, the main continuously available source on Earth are microbaroms, which are recorded globally [64, 65]. As mentioned earlier, microbaroms are generated by extended ocean wave interactions [66] which correspond to time-dependent 2d sources. Fortunately, accurate ocean wave models are already available [67]. Yet, a difficulty with such data is the need for global-scale propagation models, and the fact that their source is continuous in time, with no clear definition of arrival time as required by many inversion methods.

Numerous authors have reported balloon pressure detections of direct infrasound waves from surface explosions or seismic hammers [12, 61, 68]. However, due to the lack of dedicated seismo-acoustic experiments and the complexity of atmospheric path effects, both seismically generated epicentral infrasound and Rayleigh wave infrasound detections are still lacking, making the systematical validation of modeling and inversion methods challenging. Recent successful experiments have been piggy-backing infrasound payloads onto long-duration balloons, which reduces the deployment cost and increases the duration of pressure recordings [52, 69, 70].

(iii) Seismo-acoustic waveform modeling is crucial for investigating the sensitivity of infrasound waveforms to atmospheric and seismic parameters, especially in the absence of extensive observational datasets. In particular, for practical source and medium velocity inversions, a computationally efficient modeling of seismically-induced acoustic waves is essential to resolve microbaroms or teleseismic Rayleigh waves at regional to global scales. The few publicly available codes include the ray-tracing code InfraGA [71], the NCPAprop framework [72], and the spectral element code SPECFEM2d-DG [73, 74]. InfraGA and NCPAprop are 3d atmospheric propagation tools, while SPECFEM2d-DG is a 2d tool for simultaneous seismic and acoustic modeling. Open-source seismo-acoustic projects have seen numerous improvements in terms of usability, documentation, and implementation of new features (https://github.com/chetzer-ncpa/ncpaprop-release/, https://github.com/LANL-Seismoacoustics/infraGA and https://github.com/samosa-project/specfem2d-dg).

Fortunately, due to the large seismic-to-atmospheric impedance contrast, seismically generated infrasound propagates almost vertically as plane waves [75] with little sensitivity to horizontal wind shear. Therefore, these acoustic propagation paths can be modeled using 1d reflectivity methods [73] at low computational cost. This is not the case for other infrasound sources, such as microbaroms mentioned above, for which accurate propagation modeling requires expensive 3d simulations. Recently, Brissaud et al. [76] showed that Machine-Learning based approaches have a unique potential to speed up the propagation modeling of acoustic waves up to global distances. Additionally, other authors [28, 77] have demonstrated that the non-linear mapping between average winds, temperatures, and infrasound amplitudes and its uncertainty can be rigorously constrained purely by learning from the available data. However, more work is needed before the release of production-level tools. One of the main challenges with ML applications is to accurately predict outputs for less represented learning instances. This is particularly relevant for atmospheric sensing to probe outlier events such as Sudden Stratsopheric Warming (SSW) events, which are underrepresented in data but with significant impact on the weather [27].

(iv) In seismic inversion, key aspects in building robust source or medium property posterior distributions are: (1) availabilty of multiple seismic phases, i.e., multiple seismic stations and/or direct and reflected body and surface wave phases, (2) low seismic arrival time uncertainty, and (3) medium or source model prior uncertainty. Three-component and seismic array stations enable the identification of both seismic body-wave arrival times accurately, significantly lowering the surface-wave dispersion uncertainty. Extensive work has been done on joint inversion of direct and reflected body wave phases and surface wave dispersion curves from three-component data, e.g., in the Mars InSight mission [78, 79]. Having access to multiple phases also provides strong

constraints on source location and origin time, which is critical in the absence of a seismic catalog.

Yet, on Venus, a high-altitude TEC or pressure sensor will not measure the signal polarity and the SNR will be significantly lower than for ground recordings [52]. Venus inversions will therefore require the joint inversion of source and subsurface models from a single sensor with high uncertainties on arrival times. As mentioned earlier, Bowman et al. [13] showed that IMUs can provide direct access to polarity which would facilitate phase identification and source localization. Data uncertainties could be further reduced by deploying several sensors along a tether and applying beamforming techniques. However, wind shear will drastically increase as the tether's length increases. This limits the total length below 100 m, i.e, smaller than an acoustic wavelength at 1 Hz. Therefore, a key issue to address will be to assess the uniqueness of the inversion problem by understanding the relationships between prior uncertainties, in the Venus and source model and in the observations, and posterior Venus model distributions. Recently, Turquet and Brissaud et al. [20] provided some insight on how to leverage seismo-acoustic data for traditional seismic inversion by incorporating uncertainties using MCMC sampling and full-waveform inversion. Error prediction, even in idealized cases, will be critical in designing the next round of planetary missions.

The exploitation of seismo-acoustic datasets could lead to ground-breaking advances in weather and planetary sciences. Advances will primarily come by pushing for new dedicated experiments, improving the computational efficiency of our modeling tools, and investigating the sensitivity of infrasound waveforms to atmospheric and seismic parameters.

ACKNOWLEDGEMENTS

This work received support from the *Airborne Inversion of Rayleigh waves* (AIR) project, funded by the Research Council of Norway basic research program FRIPRO, Contract 335903.

REFERENCES

1. L. G. Evers et al. The characteristics of infrasound, its propagation and some early history. *Infrasound monitoring for atmospheric studies*, pages 3–27, 2009.
2. J. M. McKisic. Infrasound and the infrasonic monitoring of atmospheric nuclear explosions: A literature review. *AD-a339*, 249:36, 1997.
3. F. Dannemann Dugick et al. A new decade in seismoacoustics (2010–2022). *BSSA*, 04 2023.
4. C. de Groot-Hedlin et al. Detection of infrasound signals and sources using a dense seismic network. *Infrasound monitoring for atmospheric studies: Challenges in middle atmosphere dynamics and societal benefits*, pages 669–700, 2019.
5. E. M. Blixt et al. Estimating tropospheric and stratospheric winds using infrasound from explosions. *JASA*, 146(2):973–982, 2019.
6. I. Vera Rodriguez et al. Acoustic signals of a meteoroid recorded on a large-N seismic network and fiber-optic cables. *SSA*, 94(2A):731–745, 2023.
7. R. F. Garcia et al. Newly formed craters on Mars located using seismic and acoustic wave data from InSight. *Nat. Geo.*, pages 1–7, September 2022.
8. W. N. Edwards et al. Seismic observations of meteors: Coupling theory and observations. *Rev. of Geo.*, 46(4):RG4007, December 2008.
9. B. Dando et al. Exposing military attacks in the 2022 Russia-Ukraine conflict using seismic array data. *Nature*, 2023.
10. E. Astafyeva. Ionospheric detection of natural hazards. *Rev. of Geo.*, 57(4):1265–1288, 2019.
11. Y.-M. Yang et al. Satellite-based observations of tsunami-induced mesosphere airglow perturbations. *GRL*, 44(1):522–532, 2017.
12. S. Krishnamoorthy et al. Detection of artificially generated seismic signals using balloon-borne infrasound sensors. *GRL*, 45(8):3393–3403, 2018.

13. D. C. Bowman et al. Infrasound direction of arrival determination using a balloon-borne aeroseismometer. *JASA Express Letters*, 2(5):054001, May 2022.
14. J. Stevens et al. Constraints on infrasound scaling and attenuation relations from Soviet explosion data. *Monitoring the Comprehensive Nuclear-Test-Ban Treaty: Data Processing and Infrasound*, pages 1045–1062, 2002.
15. J. P. Mutschlecner et al. Infrasound from earthquakes. *Journal of Geo. Res.: Atmospheres*, 110(D1), 2005.
16. A. Le Pichon et al. Incorporating numerical modeling into estimates of the detection capability of the IMS infrasound network. *Journal of Geo. Res.: Atmospheres*, 117(D5):1–12, 2012.
17. D. N. Green et al. Infrasound signal duration: The effects of propagation distance and waveguide structure. *GJI*, 216(3):1974–1988, 2019.
18. G. Averbuch et al. Probabilistic inversion for submerged source depth and strength from infrasound observations. *JASA*, 147(2):1066–1077, 2020.
19. K. Kim et al. Seismoacoustic explosion yield and depth estimation: Insights from the large surface explosion coupling experiment. *BSSA*, 113(4):1457–1470, 2023.
20. A. Turquet et al. Retrieving seismic source characteristics using seismic and infrasound data: The 2020 mb 4.9 Kiruna minequake, Sweden. *GRL*, 2024.
21. Q. Brissaud et al. The first detection of an earthquake from a balloon using its acoustic signature. *GRL*, 48(12):e2021GL093013, 2021.
22. J. Amezcua et al. Assimilation of atmospheric infrasound data to constrain tropospheric and stratospheric winds. *QJRMS*, 146(731):2634–2653, 2020.
23. G. Averbuch et al. Evidence for short temporal atmospheric variations observed by infrasonic signals: 1. the troposphere. *ESS*, 9(3):e2021EA002036, 2022.
24. I. Vera Rodriguez et al. Atmospheric wind and temperature profiles inversion using infrasound: An ensemble model context. *J. Acoust. Soc. America*, 148(5):2923–2934, 2020.
25. J. Park et al. Atmospheric model inversion using infrasound signals from the North Korean underground nuclear explosion and the subsequent collapse event in 2017. *Geophysical Journal International*, 232(2):902–922, 2023.
26. P. Blom et al. Characteristics of thermospheric infrasound predicted using ray tracing and weakly non-linear waveform analyses. *JASA*, 149(5):3174–3188, 2021.
27. E. Vorobeva et al. Benchmarking microbarom radiation and propagation model against infrasound recordings: a vespagram-based approach. *Annales Geo.*, 39(3):515–531, 2021.
28. E. Vorobeva et al. Estimating stratospheric polar vortex strength using ambient ocean-generated infrasound and stochastics-based machine learning. *Quarterly J. Royal Meteorol. Soc.*, 2024.
29. M. D. Eggen et al. Delay-SDE-net: A deep learning approach for time series modelling with memory and uncertainty estimates, 2023. ArXiv e-print available at https://doi.org/10.48550/arXiv.2303.08587.
30. P. Lognonné et al. SEIS: Insight's seismic experiment for internal structure of Mars. *SSR*, 215(1):12, 2019.
31. W. B. Banerdt et al. Initial results from the InSight mission on Mars. *Nat. Geo.*, 13(3):183–189, March 2020.
32. D. Banfield et al. Insight auxiliary payload sensor suite (APSS). *SSR*, 215(1):4, December 2018.
33. D. Banfield et al. The atmosphere of Mars as observed by InSight. *Nat. Geo.*, 13(3):190–198, March 2020.
34. L. Martire et al. Martian infrasound: Numerical modeling and analysis of InSight's data. *Journal of Geo. Res.: Planets*, 125(6):e2020JE006376, 2020.

35. R. F. Garcia et al. Search for infrasound signals in InSight data using coupled pressure/ground deformation methods. *BSSA*, 111(6):3055–3064, October 2021.
36. I. J. Daubar et al. Two seismic events from InSight confirmed as new impacts on Mars. *TPSJ*, 4(9):175, September 2023.
37. E. T. Herrin et al. Evidence for an infrasound waveguide. *GRL*, 33(7), 2006.
38. P. T. Negraru et al. On infrasound waveguides and dispersion. *Seismological Research Letters*, 80(4):565–571, July 2009.
39. R. F. Garcia et al. Finite-difference modeling of acoustic and gravity wave propagation in Mars atmosphere: application to infrasounds emitted by meteor impacts. *SSR*, 211(1-4):547–570, 2017. Publisher: Springer.
40. Z. Xu et al. Modeling seismic recordings of high-frequency guided infrasound on Mars. *Journal of Geo. Res.: Planets*, 127(11):e2022JE007483, 2022.
41. M. Froment et al. Dispersed seismo-acoustic signals following Martian meteorite impacts: Modeling and inversion. In *AGU Fall Meeting Abstracts*, volume 2022, pages P26B–08, 2022.
42. M. Froment. *Meteorite Impacts on Mars–Seismic Observation, Source Theory and Modeling*. PhD thesis, Université Paris Cité, 2023.
43. J. P. Mutschlecner et al. Infrasound from earthquakes. *J. Geophys. Res.*, 110(D1):D01108, 2005.
44. J. B. Johnson et al. Mapping the sources of proximal earthquake infrasound. *GRL*, 47(23):e2020GL091421, 2020.
45. P. Inchin et al. Inferring the evolution of a large earthquake from its acoustic impacts on the ionosphere. *AGU Advances*, 2(2):e2020AV000260, 2021.
46. S. Shani-Kadmiel et al. The 2010 Haiti earthquake revisited: An acoustic intensity map from remote atmospheric infrasound observations. *EPSL*, 560:116795, 2021.
47. A. Le Pichon et al. Infrasound associated with 2004–2005 large Sumatra earthquakes and tsunami. *GRL*, 32(19), 2005.
48. C. Pilger et al. Infrasound and seismoacoustic signatures of the 28 September 2018 Sulawesi super-shear earthquake. *Natural Hazards & Earth System Sciences*, 19(12), 2019.
49. V. H. Lai et al. Inflation and asymmetric collapse at Kīlauea summit during the 2018 eruption from seismic and infrasound analyses. *Journal of Geo. Res.: Solid Earth*, 126(10):e2021JB022139, 2021.
50. O. A. Godin. Low-frequency sound transmission through a gas–solid interface. *JASA*, 129(2):EL45–EL51, 2011.
51. K. A. Macpherson et al. Using local infrasound to estimate seismic velocity and earthquake magnitudes. *BSSA*, 113(4):1434–1456, 2023.
52. R. F. Garcia et al. Infrasound from large earthquakes recorded on a network of balloons in the stratosphere. *GRL*, 49(15):e2022GL098844, 2022.
53. D. Fee et al. Characterizing infrasound station frequency response using large earthquakes and colocated seismometers. *BSSA*, 113(4):1581–1595, 2023.
54. L. M. Rolland et al. The resonant response of the ionosphere imaged after the 2011 off the Pacific coast of Tohoku Earthquake. *Earth, Planets and Space*, 63(7):853–857, July 2011.
55. H. Liu et al. Relating far-field coseismic ionospheric disturbances to geological structures. *Journal of Geo. Res.: Space Physics*, 126(7):e2021JA029209, 2021.
56. C. Reddy et al. Two-mode ionospheric response and Rayleigh wave group velocity distribution reckoned from GPS measurement following Mw 7.8 Nepal earthquake on 25 April 2015. *Journal of Geo. Res.: Space Physics*, 120(8):7049–7059, 2015.
57. T. Maruyama et al. Rayleigh wave signature in ionograms induced by strong earthquakes. *Journal of Geo. Res.: Space Physics*, 117(A8), 2012.

58. V. Rakoto et al. Tsunami wave height estimation from GPS-derived ionospheric data. *Journal of Geo. Res.: Space Physics*, 123(5):4329–4348, 2018.
59. Y. Cansi et al. Infrasound event detection using the progressive multi-channel correlation algorithm. In *Handbook of signal processing in acoustics*, pages 1425–1435. Springer, 2008.
60. D. Bowman et al. Geoacoustic Observations on Drifting Balloon-Borne Sensors. In A. Le Pichon et al., editors, *Infrasound Monitoring for Atmospheric Studies: Challenges in Middle Atmosphere Dynamics and Societal Benefits*, pages 125–171. Springer International Publishing, Cham, 2019.
61. R. F. Garcia et al. An active source seismo-acoustic experiment using tethered balloons to validate instrument concepts and modelling tools for atmospheric seismology. *GJI*, 225(1):186–199, February 2021.
62. J. Rouse et al. Modeling the vertical response of an aeroseismometer balloon system. Technical Report SAND2022-5405, Sandia National Lab., April 2022.
63. Y. Kakinami et al. Onset altitudes of co-seismic ionospheric disturbances determined by multiple distributions of GNSS TEC after the foreshock of the 2011 Tohoku earthquake on March 9, 2011. *Earth and Space Science*, 8(8):e2020EA001217, 2021.
64. M. Landès et al. Localization of microbarom sources using the IMS infrasound network. *Journal of Geo. Res.: Atmospheres*, 117(D6), 2012.
65. M. De Carlo et al. Global microbarom patterns: A first confirmation of the theory for source and propagation. *GRL*, 48(3):e2020GL090163, 2021.
66. M. De Carlo et al. Atmospheric infrasound generation by ocean waves in finite depth: unified theory and application to radiation patterns. *GJI*, 221(1):569–585, January 2020.
67. M. Accensi et al. ARROW. AtmospheRic inFRasound by Ocean Waves, 2024. Product User Manual.
68. D. C. Bowman et al. Acoustic event location and background noise characterization on a free flying infrasound sensor network in the stratosphere. *GJI*, 213(3):1524–1535, June 2018.
69. O. D. Lamb et al. Detecting lightning infrasound using a high-altitude balloon. *GRL*, 45(14):7176–7183, 2018.
70. G. Poler et al. Infrasound and gravity waves over the Andes observed by a pressure sensor on board a stratospheric balloon. *Journal of Geo. Res.: Atmospheres*, 125(6):e2019JD031565, 2020.
71. LANL. InfraGA/GeoAc [Software]. Los Alamos National Laboratory (LANL), 2014. Last accessed 16 May 2023.
72. R. Waxler et al. NCPAprop v2.1.0, September 2021.
73. Q. Brissaud et al. Hybrid Galerkin numerical modelling of elastodynamics and compressible Navier–Stokes couplings: applications to seismo-gravito acoustic waves. *GJI*, 210(2):1047–1069, August 2017.
74. L. Martire et al. SPECFEM2D-DG, an open-source software modelling mechanical waves in coupled solid–fluid systems: the linearized Navier–Stokes approach. *GJI*, 228(1):664–697, 2022.
75. L. Martire et al. Numerical simulation of the atmospheric signature of artificial and natural seismic events. *Geophys. Res. Lett.*, 45(21), November 2018.
76. Q. Brissaud et al. Predicting infrasound transmission loss using deep learning. *GJI*, 232(1):274–286, January 2023.
77. M. D. Eggen et al. Stochastic modeling of stratospheric temperature. *Mathematical Geosciences*, 54(4):651–678, 2022.
78. M. Drilleau et al. Structure of the Martian crust below insight from surface waves and body waves generated by nearby meteoroid impacts. *GRL*, 50(23):e2023GL104601, 2023.
79. S. Carrasco et al. Constraints for the Martian crustal structure from Rayleigh waves ellipticity of large seismic events. *GRL*, 50(16):e2023GL104816, 2023.